Journal of Power Sources 210 (2012) 32–37

Contents lists available at SciVerse ScienceDirect

Journal of Power Sources

journal homepage: www.elsevier.com/locate/jpowsour

Short communication

Hematite modified tungsten trioxide nanoparticle photoanode for solar water oxidation

Aiming Mao[a], Jung Kyu Kim[a,b], Kahee Shin[a], Dong Hwan Wang[a,b], Pil J. Yoo[a,b], Gui Young Han[a], Jong Hyeok Park[a,b,*]

[a] School of Chemical Engineering, Sungkyunkwan University, Suwon 440-746, Republic of Korea
[b] Sungkyun Advanced Institute of Nanoscience and Nanotechnology, Sungkyunkwan University, Suwon 440-746, Republic of Korea

ARTICLE INFO

Article history:
Received 23 December 2011
Received in revised form 20 February 2012
Accepted 22 February 2012
Available online 6 March 2012

Keywords:
Water splitting
Photoelectrochemical cells
Hematite
Tungsten trioxide
Nanocomposites

ABSTRACT

Hematite (α-Fe_2O_3) film is electrochemically deposited onto the surface of tungsten trioxide (WO_3) nanoparticulate film. The synthesis of the WO_3 nanostructure is directed by surfactants for control of its morphology. The resulting composite shows visible light harvesting and is tested as photoanodes in heterojunction photoelectrochemical cells for the possibility of direct water splitting under visible illumination. The composite's structural and optical properties are characterized by FESEM, EDS, XRD, XPS, and UV–vis spectrometry; its photocurrent responses are also investigated under simulated solar illumination. Coupling WO_3 with hematite results in over 9 times greater photocurrent density than that shown by pure WO_3 in sodium sulfate electrolyte. This simple modification can significantly improve the performance of WO_3.

1. Introduction

Solar energy is a cleaner, renewable alternative to fossil fuels, with wide potential applicability. However, its direct use in such as solar thermal power or photovoltaic solar cells is still limited and large scale use of solar energy requires efficient energy storage. Since Fujishima and Honda's 1977 finding that a TiO_2 photoanode in a photoelectrochemical cell (PEC) could split water into hydrogen and oxygen under UV irradiation [1], solar hydrogen generation by water splitting has been considered one of the most suitable methods of solar energy conversion and storage [2]. However, such water splitting still faces many challenges, particularly because of its low efficiency. New materials with smaller bandgaps than TiO_2 have therefore been explored so as to increase solar absorption to include visible wavelengths. Examples of photoanodes tested for PECs include metal oxide semiconductors such as tungsten trioxide (WO_3) [3–6] and iron oxide (Fe_2O_3) [7]. Interfacial effects significantly affect charge transport and research has aimed to optimize electron transport pathways through the synthesis of nanostructured photoanodes incorporating such as nanotubes [8–11], nanowires [12,13], nanosheets [14], or nanorods [15–17].

Heterojunction photoanodes can also potentially improve cells' efficiency. Heterojunction electrodes contain a small-bandgap semiconductor, such as CdS or CdSe, and a large-bandgap semiconductor, such as TiO_2 [18–20]. Unfortunately, most low-bandgap materials suffer from poor long-term stability in aqueous solution under solar illumination. α-Fe_2O_3 has a favorable bandgap of 2.0–2.2 eV, is stable against corrosion in aqueous environments at pH > 3, and is inexpensive. It is therefore a promising light absorber for heterojunction photoanodes, but is limited by poor electrical conductivity and a short minority carrier diffusion length. α-Fe_2O_3 decorated TiO_2 nanotube arrays have been reported as photoanodes for PECs, though the enhancement of photocurrent was limited because the conduction energy band of TiO_2 is higher than that of α-Fe_2O_3, which hindered electron transfer from the α-Fe_2O_3 to the TiO_2 nanotube arrays after the absorption of photons. WO_3 is a promising alternative host material for heterojunction PEC as its conduction band is only slightly lower than that of α-Fe_2O_3 [3,21,22], allowing efficient electron transport across the interface between them. Therefore, the heterojunction of α-Fe_2O_3 and WO_3 was investigated in this study (Fig. 1).

Few papers have reported α-Fe_2O_3/WO_3 photoanodes for improving the efficiency of PECs [23,24], and no noticeable photocurrent enhancement has yet emerged. This work reports the synthesis of a transparent and nanostructured α-Fe_2O_3/WO_3 film prepared in two steps. Spherical WO_3 nanoparticles were grown as a film on FTO glass by a surfactant-assisted sol–gel reaction [25]. α-Fe_2O_3 was then electrodeposited onto the WO_3 film. Pure WO_3 and

* Corresponding author at: School of Chemical Engineering, Sungkyunkwan University, Suwon 440-746, Republic of Korea. Tel.: +82 31 290 7346; fax: +82 31 290 7272.
E-mail addresses: lutts@skku.edu, anotherpark@gmail.com (J.H. Park).

0378-7753/$ – see front matter © 2012 Elsevier B.V. All rights reserved.
doi:10.1016/j.jpowsour.2012.02.112

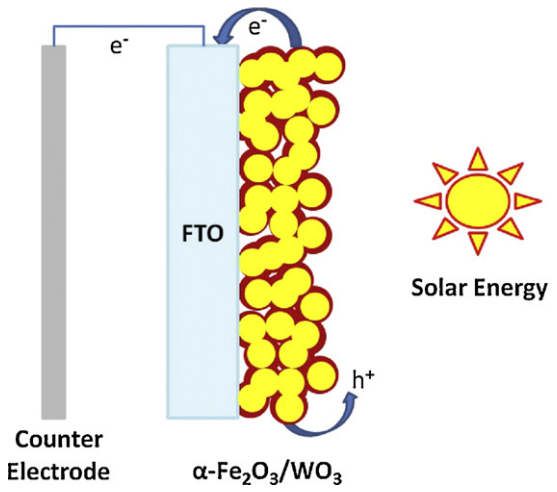

Fig. 1. Energy band diagram of α-Fe_2O_3/WO_3 film on FTO substrate.

pure α-Fe_2O_3 films were also synthesized and tested for comparison. The deposition conditions of the α-Fe_2O_3 were optimized with respect to photocurrent density, which was 9 times greater photocurrent density than that shown by pure WO_3 in sodium sulfate electrolyte.

2. Experimental

2.1. Synthesis of WO_3 nanostructured film

Nanostructured WO_3 films were deposited on transparent conducting glass substrates (F-doped SnO_2-coated glass, FTO, dimension: 1.5 cm × 1.5 cm, WOOYANGGMS, Siheung, Gyeonggi-do, Korea) using a precursor solution comprising a colloidal complex of peroxy-tungstic acid and polyethylene glycol 300, an organic stabilizer and morphology controlling agent [26]. The peroxy-tungstate precursor was prepared by mixing tungsten powder (W, 99.9%, Acros, Geel, Belgium) in hydrogen peroxide (30% H_2O_2, Junsei, Tokyo, Japan). 0.9 g tungsten was added to 10 ml H_2O_2. After 6 h, 25 ml IPA (2-propanol, Junsei, Tokyo, Japan) stabilizer and PEG 300 (polyethylene glycol 300, Aldrich, St Louis, Mo, United States) structure enhancer were added [27]. IPA can slow the condensation of tungstate [28] and can complex with tungsten oxoanions [29]. The nanostructured WO_3 films on the FTO were obtained by dropping 20 μl precursor onto the FTO substrate and drying it at room temperature for 20 min. Such dropping and drying were repeated twice more. The deposited precursor was then annealed at 550 °C for 30 min, resulting in monoclinic WO_3 (crystalline *m*-WO_3) with improved nano-crystallinity [30]. Samples were prepared with tungsten and PEG 300 at a 1:10 weight ratio.

2.2. Synthesis of α-Fe_2O_3/WO_3 nanostructured film

Fe was electrodeposited onto the WO_3 nanostructured film under a constant potential. The electrolyte was prepared by mixing 60 g ferrous sulfate ($FeSO_4 \cdot 7H_2O$, 98.0%, Junsei, Tokyo, Japan), 1.5 g ascorbic acid ($C_6H_8O_6$, 99%, Aldrich, St Louis, Mo, United States), 0.5 g amidosulfonic acid (H_2NSO_3H, 99.99%, Aldrich, St Louis, Mo, United States) and 15 g boric acid (H_3BO_3, 99.99%, Aldrich, St Louis, MO, United States) in 1 l distilled water [31]. A constant −0.5 V potential *vs.* Ag/AgCl was applied to the working electrode. Samples were then thermal annealed under air at 500 °C for 6 h to form crystalline α-Fe_2O_3/WO_3.

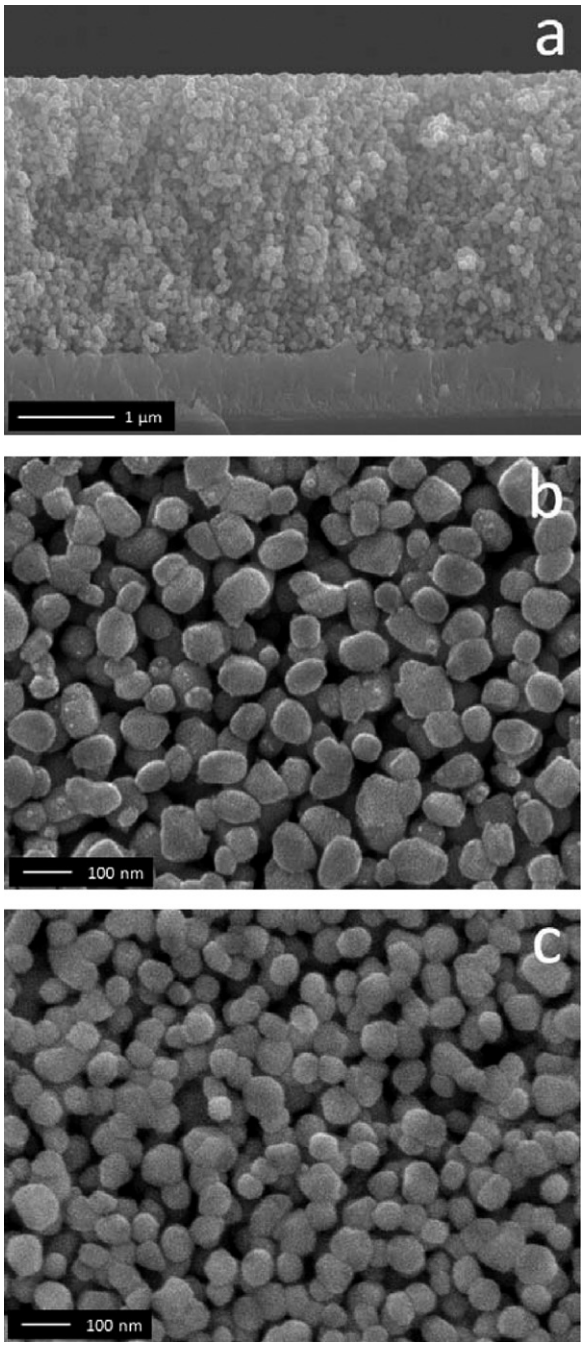

Fig. 2. FESEM images: (a) section and (b) top views of pure WO_3 film on FTO glass, (c) top view of α-Fe_2O_3/WO_3 film.

2.3. Characterization methods

Field emission scanning electron microscopy (FE-SEM, JSM-7000F, JEOL Co., Tokyo, Japan) was used to examine the samples' morphologies. Energy dispersive spectrometry (EDS, Oxford, INCA, Oxfordshire, United Kingdom) was used to identify constituent elements and their distributions. X-ray diffraction spectra were recorded to observe crystalline phases on a Siemens diffractometer D500/5000 in Bragg-Bretano geometry using Cu Kα radiation (D500/5000, Bruker, Billerica, MA, United States). X-ray photoelectron spectroscopy (XPS) was conducted on an AES-XPS instrument (ESCA2000, VG Microtech, West Sussex, United Kingdom) with an aluminum anode (Al Kα = 1486.6 eV). Optical properties were

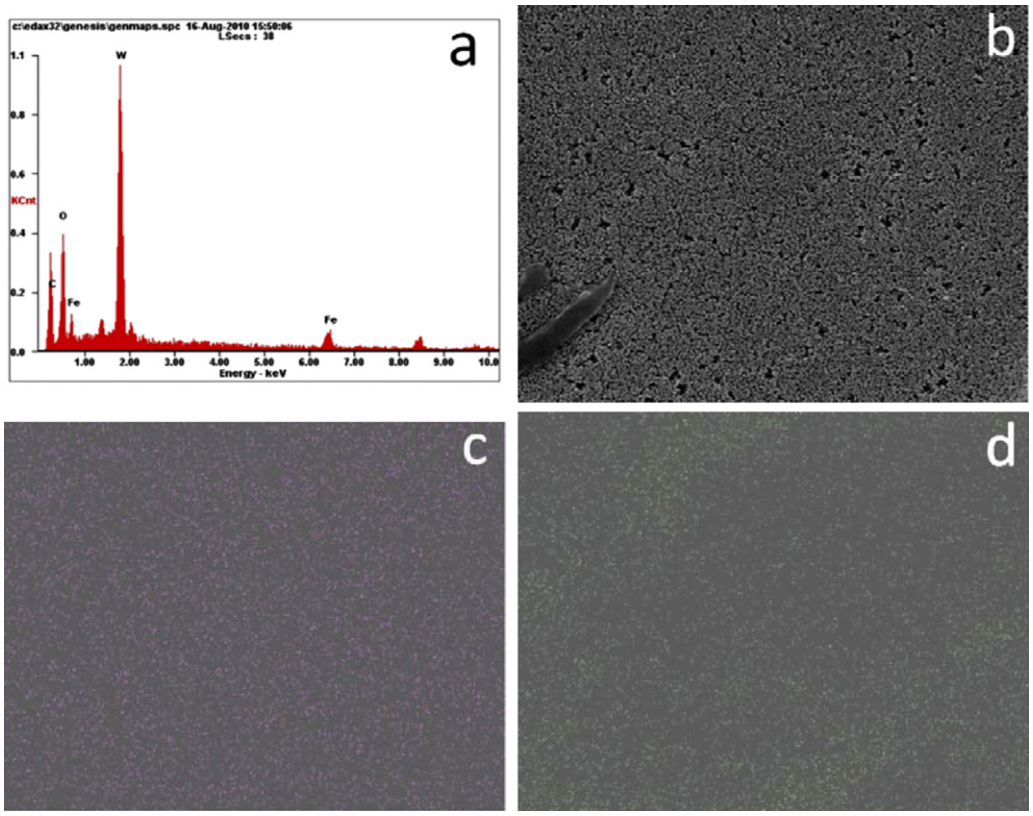

Fig. 3. Energy dispersive spectroscopy data of α-Fe_2O_3/WO_3 film: (a) elemental analysis, (b) FESEM image of α-Fe_2O_3/WO_3 film, (c) tungsten elemental mapping corresponding to Fig. 2b, (c) iron element mapping corresponding to Fig. 2b.

investigated by UV–vis spectrophotometry (UV-2401 PC, Shimadzu, Koyoto, Japan).

2.4. Photoelectrochemical measurements

Samples' photoelectrochemical properties were investigated in a typical three-electrode configuration using a Pt plate counter electrode, an Ag/AgCl (CHI 660, CH Instruments, Austin, Texas, United States) reference electrode, and 0.2 M aqueous sodium sulfate (Na_2SO_4, 98.0%, Junsei, Tokyo, Japan) electrolyte. Linear sweep voltammetry was conducted at a scan rate of 20 mV s^{-1}. Each sample, as the working electrode, was illuminated under AM 1.5 G (100 mW$(cm^2)^{-1}$) light from a 150 W xenon lamp (with AM 1.5 G filter) solar simulator (PEC-L01, PECCELL, Yokohama, Japan). The light intensity was calibrated using a reference cell (Certificate no. C-ISE269, Fraunhofer ISE, Freiburg, Germany). Incident photon to current efficiency (IPCE) was measured using a 300 W xenon light source and a monochromator (Polaronix K3100 IPCE Measurement System, McScience, Suwon, Gyeonggi-do, Korea).

3. Results and discussion

Section- and top-view FE-SEM images of the WO_3 nanoparticle film (Fig. 2a and b) shows uniformly agglomerated WO_3 nanoparticles of 40–100 nm diameter in a film of *ca.* 3 μm thickness. This nanoporous structure provided a large contact area between the electrolyte and the WO_3 nanoparticles, which could increase light absorption and decrease recombination between photo-excited electrons and holes. This nanoporous structure also allowed α-Fe_2O_3 to be uniformly dispersed into it (Fig. 2c), with no obvious differences shown by FESEM after the deposition of α-Fe_2O_3. EDS identified the presence of Fe at *ca.* 6.73 wt.%. Elemental analysis of the α-Fe_2O_3/WO_3 film (Fig. 3a) and elemental mappings of tungsten (Fig. 3c) and iron (Fig. 3d), in the areas corresponding the FESEM image in Fig. 3b show that Fe was uniformly distributed over the whole region, demonstrating the good dispersion of the α-Fe_2O_3 in the WO_3 film. Such a well mixed composite could show extended absorption wavelengths due to the α-Fe_2O_3 and increased electron transport due to the WO_3 backbone. And elemental mapping of cross section is showed in Fig. S1.

XRD patterns of the nanostructured α-Fe_2O_3/WO_3 film were recorded to assess the composite's phase and crystalline properties (Fig. 4). The peaks due to the FTO substrate were indexed to SnO_2 at 26.5°, 34.2°, 37.7° and 51.4° (JCPDS no. 41-1445). The strongest diffraction peaks at 23.6°, 24.4°, 34°, 48.2°, and 49.8° were attributed to monoclinic WO_3 (JCPDS no. 43-1035). The peaks at 22°, 34° and 56° indicate rhombohedral Fe_2O_3 (JCPDS no. 24-0072). The weak peaks of α-Fe_2O_3 were due to its low concentrations in

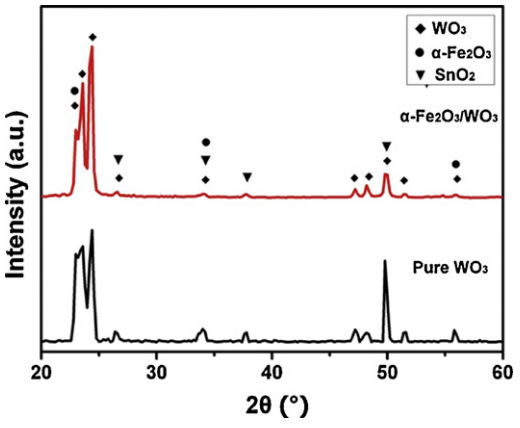

Fig. 4. X-ray diffraction patterns of pure WO_3 film and α-Fe_2O_3/WO_3 film.

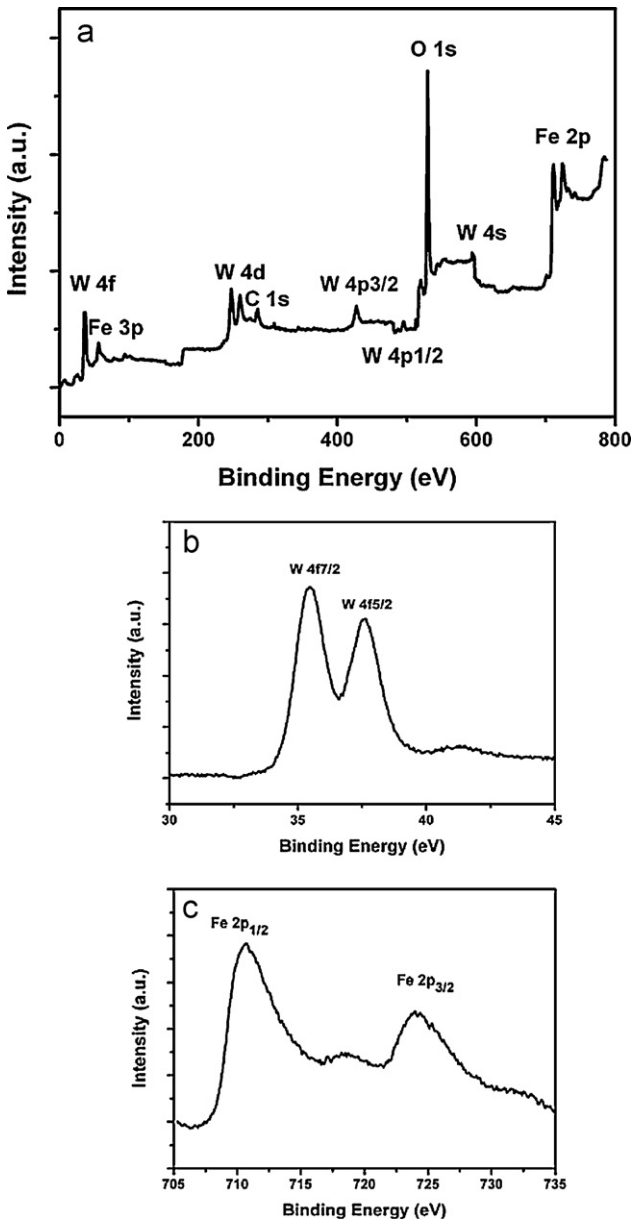

Fig. 5. X-ray photoelectron spectroscopy analysis of α-Fe_2O_3/WO_3 film: (a) wide scan, (b) narrow scan for tungsten element, (c) narrow scan for iron element.

the samples. The formation of such as $FeWO_4$ or Fe_2WO_6 was not observed in the XRD patterns. XPS was used to assess the composition of the α-Fe_2O_3/WO_3 film (Fig. 5a): the sample's surface contained W, Fe, O and C elements, with the presence of carbon attributable to carbonized organic material remaining after the thermal annealing. Higher resolution spectra of tungsten (Fig. 5b) and iron (Fig. 5c) were recorded to examine their oxidation states. The W 4f7/2 and W 4f5/2 peaks at 35.5 and 37.6 eV were due to W–O bonds in WO_3 [32]. The binding energies of Fe 2p3/2 and Fe 2p1/2 were 711.0 and 725.0 eV, respectively, matching closely those previously reported for Fe^{3+} in α-Fe_2O_3 [33,34].

Optical properties of the samples were characterized by UV–Vis spectroscopy (Fig. 6a). Reflectance by pure WO_3 film sharply decreased at *ca.* 460 nm, corresponding to a band gap of *ca.* 2.7 eV. α-Fe_2O_3/WO_3 film showed an onset of absorbance at *ca.* 600 nm, implying a bandgap of *ca.* 2.0 eV. Solar absorption was expanded from 480 to 600 nm by the introduction of α-Fe_2O_3 to the WO_3 film. Photocurrents *vs.* potential of samples (*I–V*, Fig. 6b) were measured in 0.2 M Na_2SO_4 electrolyte. Detailed information about onset potentials are shown in Fig. S1. The dark currents of the samples were very similar. The photocurrent densities increased with the applied potential under the AM 1.5 G solar illumination. The photocurrent density of the α-Fe_2O_3/WO_3 film was consistently much higher than that of pure WO_3 film, likely due to the synergy of improved solar absorption and better charge transportation in the heterojunction of α-Fe_2O_3 and WO_3. The photocurrent responses of the α-Fe_2O_3/WO_3 films were assessed with respect to their composition by varying the duration of Fe deposition: 6 s, 10 s, and 20 s, at −0.5 V *vs.* Ag/AgCl in the given electrolyte (see Section 2). Deposition for 10 s resulted in the highest photocurrent density of *ca.* 0.91 mA$(cm^2)^{-1}$, *ca.* 50 times that of any previously reported value for this composite [23]. Similar photocurrent densities have previously been observed in a basic electrolyte of NaOH solution [24], though WO_3 is not stable in basic solutions. The reaction between WO_3 and NaOH can strongly influence the validity of the photocurrent density. A theoretical expression of photocurrent density can explain the compositional effects of the α-Fe_2O_3/WO_3 film. The photocurrent is proportional to the amount of photoelectrons produced by a semiconductor's absorption of light that can pass through a circuit to the counter electrode. An initial increasing of α-Fe_2O_3 content (for example in the sample made with Fe deposition for 10 s), allows greater generation of photoelectrons and hence increased photocurrent density. A further increase of α-Fe_2O_3 in the nanoporous WO_3 nanoparticle film, after Fe deposition for 20 s, likely reduced the contact area between the sample and the electrolyte, increasing charge recombination in the α-Fe_2O_3 due to its short exciton diffusion length. Therefore, if the α-Fe_2O_3 content exceeds a critical amount, the photocurrent density of the composite will decrease. Chronoamperometry of the WO_3 film with Fe deposited for 10 s was conducted to observe the stability of its photo-response. Under chopping AM 1.5 G light, the sample showed strong responses to the light. The photocurrent density decreased slightly over 300 s, though it remained very high, *ca.* 0.8 mA$(cm^2)^{-1}$ after 300 s of illumination (Fig. 6c).

The overall solar-to-hydrogen conversion efficiency of a PEC, η, for the water splitting reaction can be determined by Eq. (1) [35], assuming that all the photocurrent that passes through the circuit participates in the water splitting reaction:

$$\eta\ (\%) = \frac{j_p \times (1.23 - E_{app})}{P_{light}} \quad (1)$$

where the photocurrent density, j_p, is in mA$(cm^2)^{-1}$, E_{app} is the bias voltage applied within the working electrode and counter electrode to assist the water splitting reaction, and P_{light} is the intensity of solar irradiation in mW$(cm^2)^{-1}$. To obtain the E_{app}, a two-electrode configuration was used, in which the tested samples were the working electrode and a Pt plate acted as the counter electrode. At P_{light} = 100 mW$(cm^2)^{-1}$, photoconversion efficiency was optimized at *ca.* 0.5% under an applied potential of 0.6–0.7 V (Fig. 6d).

To verify the photocurrent at 0.6 V *vs.* Ag/AgCl, the incident photon to current conversion efficiency (IPCE) was examined at wavelengths of 300–700 nm (Fig. 6e). Pure WO_3 showed a strong photon response at 300–460 nm, indicating a bandgap of *ca.* 2.7 eV. The α-Fe_2O_3/WO_3 films showed higher IPCE values with absorption extended to 620 nm, indicating a bandgap of *ca.* 2.0 eV. The WO_3 film depostited with Fe for 10 s showed the highest IPCE of over 25% at 360 nm, which gradually decreased to zero at 620 nm. The large increase of IPCE indicates that the heterojunction of α-Fe_2O_3 and WO_3 was better at harvesting incident photons to induce water splitting. The solar photocurrent spectrum (J_{spec}) is the product of the IPCE and the photon flux of the AM 1.5 G light and when integrated gives a value of the photocurrent, the integrated

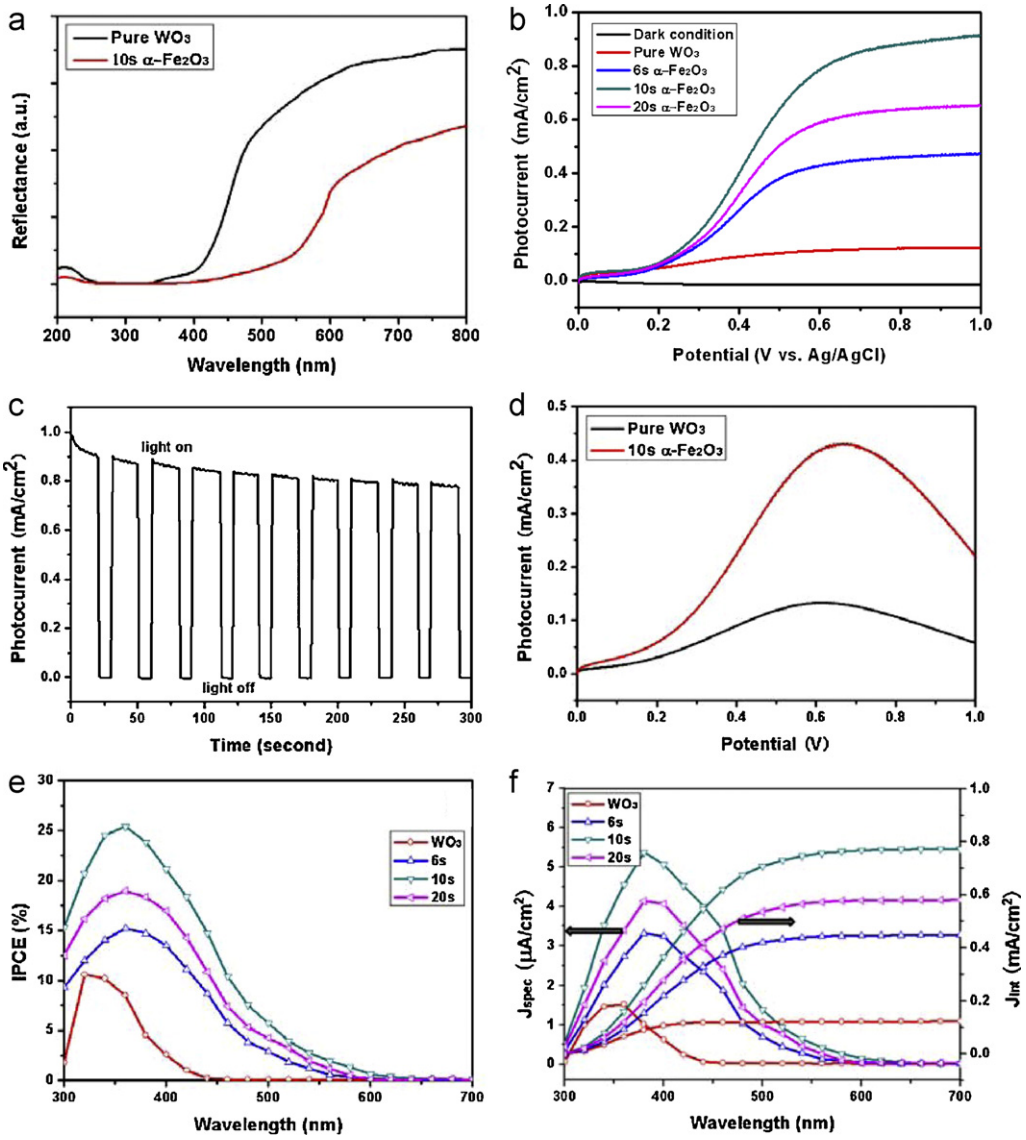

Fig. 6. Photoelectrochemical characterizations of pure WO_3 and α-Fe_2O_3/WO_3 films under AM 1.5 G illumination: (a) UV–vis reflection spectra; (b) photocurrent–potential (*I–V*) responses of samples in 0.2 M Na_2SO_4 electrolyte; (c) chronoamperometry of WO_3 film with 10 s α-Fe_2O_3 deposition at 1.0 V applied potential *vs.* Ag/AgCl under light chopping; (d) overall solar-to-hydrogen conversion efficiency measured in two-electrode configuration, with samples as photoanodes, Pt plate as counter electrode, and 0.2 M aqueous Na_2SO_4 electrolyte; (e) incident photon to current conversion efficiency; (f) solar photocurrent spectra (J_{spect}) and integrated solar photocurrent (J_{int}).

solar photocurrent (J_{int}). The integrated solar photocurrent of the WO_3 film deposited with α-Fe_2O_3 for 10 s was 0.77 mA$(cm^2)^{-1}$ (Fig. 6f), very close to the mA$(cm^2)^{-1}$ measured in the *I–V* study. Photocurrent densities and integrated photocurrents are listed in Table S1 of the supporting information.

4. Conclusions

A nanostructured α-Fe_2O_3/WO_3 film with a nanoporous morphology was prepared and investigated for the photoelectrochemical splitting of water. The heterojunction of α-Fe_2O_3 and WO_3 appeared promising for improved water splitting performance. UV–vis reflectance measurements showed that absorption wavelengths increased from 480 to 600 nm after coating α-Fe_2O_3 onto the WO_3 nanoparticle film. Photocurrent potential and incident photon to current conversion efficiency measurements showed that the photo-response of α-Fe_2O_3/WO_3 film under AM 1.5 G illumination was much higher than that of pure WO_3 film, indicating that the heterojunction of α-Fe_2O_3 and WO_3 enhanced light absorption and transport of photogenerated charges. The deposition conditions of the Fe oxide on the WO_3 nanoparticle film were optimized. The maximum photocurrent density of the photoanode was 0.91 mA$(cm^2)^{-1}$ and the highest overall solar-to-hydrogen conversion efficiency of the PEC was about *ca.* 0.5% at 0.6–0.7 V *vs.* Pt.

Acknowledgements

This work was supported by grants (2011-0030254 and NCRC program (2011-0006268)) of National Research Foundation (NRF) funded by the Korea Ministry of Education, Science and Technology (MEST). J. H. Park acknowledges Future-based Technology Development Program (Nano Fields) through the National Research Foundation of Korea (NRF) funded by the Ministry of Education, Science and Technology (2010-0029321). A. Mao and J. K. Kim contributed equally to this work.

Appendix A. Supplementary data

Supplementary data associated with this article can be found, in the online version, at doi:10.1016/j.jpowsour.2012.02.112.

References

[1] A. Fujishima, K. Honda, Nature 238 (1971) 37.
[2] Z.G. Zou, J.H. Ye, H. Arakawa, Nature 414 (2001) 625.
[3] C. Santato, M. Ulmann, J. Augustynski, J. Phys. Chem. B 105 (2001) 936.
[4] A. Enesca, A. Duta, J. Schoonman, Thin Solid Films 515 (2007) 6371.
[5] B. Yang, Y.J. Zhang, E. Drabarek, P.R.F. Barnes, V. Luca, Chem. Mater. 19 (2007) 5664.
[6] M. Yagi, S. Maruyama, K. Sone, K. Nagai, T. Norimatsu, J. Solid State Chem. 181 (2008) 181.
[7] S.U.M. Khan, J. Akikusa, J. Phys. Chem. B 103 (1999) 7184.
[8] G.K. Mor, K. Shankar, M. Paulose, O.K. Varghese, C.A. Grimes, Nano Lett. 5 (2005) 191.
[9] N.K. Allam, K. Shankar, C.A. Grimes, J. Mater. Chem. 18 (2008) 2341.
[10] Q.Q. Chen, D.S. Xu, Z.Y. Wu, Z.F. Liu, Nanotechnology 19 (2008) 5.
[11] E.Y. Kim, J.H. Park, G.Y. Han, J. Power Sources 184 (2008) 284.
[12] S.U.M. Khan, T. Sultana, Sol. Energy Mater. Sol. Cells 76 (2003) 211.
[13] M. Kitano, R. Mitsui, D.R. Eddy, Catal. Lett. 119 (2007) 217.
[14] I. Cesar, A. Kay, J.A.G. Martinez, M. Gratzel, J. Am. Chem. Soc. 128 (2006) 4582.
[15] A. Wolcott, W.A. Smith, T.R. Kuykendall, Y. Zhao, J.Z. Zhang, Small 5 (2009) 104.
[16] A. Mao, G.Y. Han, J.H. Park, J. Mater. Chem. 20 (2010) 2247.
[17] A. Mao, N.G. Park, G.Y. Han, J.H. Park, Nanotechnology 22 (2011) 175703.
[18] K.H. Shin, S.I. Seok, S.H. Im, J.H. Park, Chem. Commun. 46 (2010) 2385.
[19] M. Tomkiewicz, J.M. Woodall, J. Electrochem. Soc. 124 (1977) 1436.
[20] P.A. Kohl, S.N. Frank, A.J. Bard, J. Electrochem. Soc. 124 (1977) 225.
[21] H. Wang, T. Lindgren, J. He, A. Hagfeldt, S.E. Lindquist, J. Phys. Chem. B 104 (2000) 5686.
[22] R. Van De Krol, Y. Liang, J. Schoonman, J. Mater. Chem. 18 (2008) 2311.
[23] W. Luo, T. Yu, Y. Wang, Z. Li, J. Ye, Z. Zou, J. Phys. D: Appl. Phys. 40 (2007) 1091.
[24] K. Sivula, F.L. Formal, M. Gratzel, Chem. Mater. 21 (2009) 2862.
[25] J.K. kim, K. Shin, S.M. Cho, T.W. Lee, J.H. Park, Energy Environ. Sci. 4 (2011) 1465.
[26] R. Solarska, C. Santato, C. Jorand-Sartoretti, M. Ulmann, J. Augustynski, J. Appl. Electrochem. 35 (2005) 715.
[27] C. Santato, M. Ulmann, J. Augustynski, Adv. Mater. 13 (2001) 511.
[28] L. Jean, L. Jean, Can. J. Chem. 55 (1977) 3758.
[29] E. Richardson, J. Inorg. Nucl. Chem. 12 (1959) 79.
[30] C. Santato, M. Odziemkowski, M. Ulmann, J. Augustynski, J. Am. Chem. Soc. 123 (2001) 10639.
[31] Y. Wang, S. Wang, W. Zhao, B. Zhu, F. Kong, D. Wang, S. Wu, W. Huang, S. Zhang, Sens. Actuators B 125 (2007) 79.
[32] Q. Zhang, A.K. Chakraborty, W.I. Lee, Bull. Korean Chem. Soc. 30 (2009) 227.
[33] P. Bera, K.R. Priolkar, A. Gayen, Chem. Mater. 15 (2003) 2049.
[34] C.J. Sartoretti, M. Ulmann, B.D. Alexander, J. Augustynski, Chem. Phys. Lett. 376 (2003) 194.
[35] S.K. Mohapatra, S. Banerjee, M. Misra, Nanotechnology 19 (2008) 315601.